solids

MDPI

Article

Synthesis, Structural Characterization, Conformational and Topological Classification of Different Salts in the 2,2-Dimethylpropane-1,3-diamine/HCl/H_2O-System

Jaqueline Heimgert [1], Florian Morsbach [1], Martin Kleinschmidt [2] and Guido J. Reiss [1,*]

[1] Institut für Anorganische Chemie und Strukturchemie, Lehrstuhl II Material-und Strukturforschung, Heinrich-Heine-Universität Düsseldorf, Universitätsstraße 1, D-40225 Düsseldorf, Germany; jaqueline.heimgert@hhu.de (J.H.); florian.morsbach@hhu.de (F.M.)

[2] Institut für Theoretische Chemie und Computerchemie, Heinrich-Heine-Universität Düsseldorf, Universitätsstraße 1, D-40225 Düsseldorf, Germany; martin.kleinschmidt@hhu.de

* Correspondence: reissg@hhu.de

Abstract: The reaction of 2,2-dimethylpropane-1,3-diamine (*dmpn*) with an excess of concentrated aqueous hydrochloric acid yielded colorless crystals of 2,2-dimethylpropane-1,3-diaminium dichloride, *dmpn*H_2Cl_2 (**1**), in addition to small amounts of a monohydrate, *dmpn*$H_2Cl_2 \cdot H_2O$ (**2**). The compounds were studied via X-ray crystallography, IR and Raman spectroscopy, NMR spectroscopy and thermal analysis. Single crystal structure determinations on **1** and **2** showed that *dmpn*H_2Cl_2 exists in two polymorphic forms, **1a** and **1b**. The crystal structure of **1b** showed to be much more complex than that of **1a**. In the crystal structure of **2**, four $(dmpnH_2)^{2+}$ cations and eight chloride anions form a cage constructed by N−H···Cl hydrogen bonds. In the center of these cages water dimers with a O···O distance of 2.776 (8) Å are present. In addition, a conformational analysis of the 2,2-dimethylpropane-1,3-diaminium cation was performed. The results are compared to the experimental findings of **1a**, **1b**, **2** and other related hydrogen bonded salt structures from the Cambridge crystallographic structure database (CCDC). Last, a topological classification of the solid-state structures of **1a** and **2** was performed and the simplified topological networks are discussed.

Keywords: X-ray crystallography; polymorphs; hydrogen bonding; cage structure; water dimers; conformational analysis; topological classification

Citation: Heimgert, J.; Morsbach, F.; Kleinschmidt, M.; Reiss, G.J. Synthesis, Structural Characterization, Conformational and Topological Classification of Different Salts in the 2,2-Dimethylpropane-1,3-diamine/HCl/H_2O-System. *Solids* **2022**, *3*, 385–396. https://doi.org/10.3390/solids3030027

Academic Editor: Maija Nissinen

Received: 9 May 2022
Accepted: 16 June 2022
Published: 28 June 2022

1. Introduction

Generally, 2,2-dimethylpropane-1,3-diamine (*dmpn*) is easily accessible through the reduction of 1,3-dinitro-2,2-dimethylpropane with iron in high yields [1]. The synthetic protocol of *dmpn* has been optimized and was applied for patent in 1973 [2]. With transition metals *dmpn* forms stable complexes [3–6]. Consequently, *dmpn* and ligands with a similar topology have a broad scope application such as their use as bridging ligands in metal organic frameworks and in coordination polymers [7,8]. Recently we reported the interesting finding that *dmpn* is able to capture CO_2 spontaneously by the formation of (3-ammonio-2,2-dimethyl-propyl)carbamate dihydrate [9]. The carbamate releases its CO_2 on heating which might add some applications.

The crystal structures of different salt-like compounds containing the di-protonated *dmpn* are accessible [7,10–17]. In total sixteen related structures can be found in the CSD [18]. Since the crystal structures of *dmpn* dihydrobromide [11], *dmpn* dihydroiodide [11] as well as *dmpn* dihydroiodide−iodide (1/1) have already been determined [12] it is wondrous that no crystal structure of the respective dihydrochloride has been published until now. We were able to characterize three different phases in the *dmpn*/HCl/H_2O-system (Figure 1). The crystal structures of two polymorphic forms of *dmpn* dihydrochloride (**1a** and **1b**), and of *dmpn* dihydrochloride monohydrate (**2**), have been determined. The structures

of **1a** and **1b** differ strongly from each other and **1a** will be discussed in detail, while **1b** only has been deposited as a CSD communication [19], as its structure turned out to be very complex, with a large *Z* and a hydrogen bonded network that does not easily fit into a simple architecture of hydrogen bonds [20,21]. To get an impression of the forces that mainly contribute to the solid-state structures containing the 2,2-dimethylpropane-1,3-diaminium cation [$(dmpnH_2)^{2+}$], a conformational analysis was performed to compare the intramolecular interactions in terms of intermolecular interactions such as charge supported hydrogen bonding and van der Waals forces in the crystal structures of: $dmpnH_2Cl_2$ (**1a** and **1b** [19]), $dmpnH_2Cl_2{\cdot}H_2O$ (**2**), $dmpnH_2Br_2$ [11], $dmpnH_2I_2$ [11], $dmpnH_2I_2I_2$ [12], $dmpnH_2(NO_3)_2$ [13], $dmpnH_2(CrO_4)$ [14], $dmpnH_2[ZnCl_4]$ [15], $dmpnH_2[CdBr_4]$ [16], and $dmpnH_2[InBr_4][InBr_{11}]$ [17].

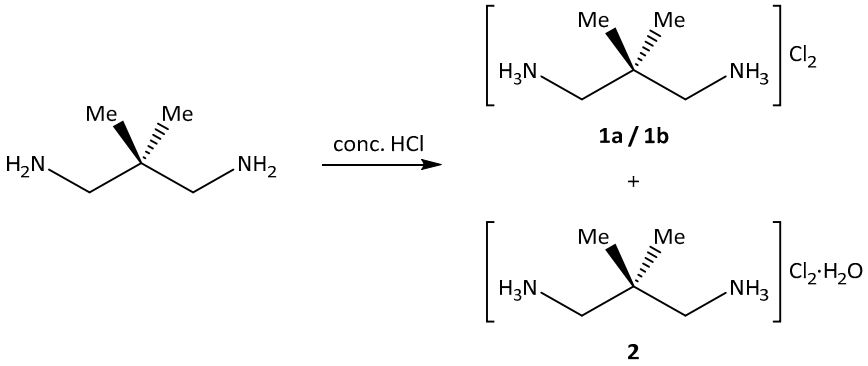

Figure 1. Formation of the three salts in the 2,2-dimethylpropane-1,3-diamine/HCl/H_2O-system described in this work: 2,2-dimethylpropane-1,3-diaminium dichloride (**1a** and **1b**), $dmpnH_2Cl_2$, and 2,2-dimethylpropane-1,3-diaminium dichloride monohydrate (**2**), $dmpnH_2Cl_2{\cdot}H_2O$.

2. Materials and Methods

2.1. Synthesis

All chemicals were obtained from commercial sources and used as purchased. 10 mL of conc. hydrochloric acid (~120 mmol) was added dropwise to 3.07 g of 2,2-dimethylpropane-1,3-diamine (30 mmol). After complete neutralization of the amine by the hydrochloric acid, the HCl concentration in the obtained solution was approximately 6 $mol{\cdot}L^{-1}$. This clear, colorless solution was left in a fume hood for two weeks until the liquid had completely evaporated. Yield: 4.83 g = 92% (calc. for $C_5H_{16}N_2Cl_2$), colorless solid. A CHN analysis was performed with a *vario MICRO cube* [22]. Analysis calculated for $C_5H_{16}N_2Cl_2$ [%]: C 34.30, H 9.21, N 16.00; found: C 34.12, H 9.09, N 15.74. ^{1}H- and $^{13}C\{^1H\}$-NMR-spectra were recorded with a *Bruker Avance III* spectrometer and analyzed with the *MestReNova* software package [23]. ^{1}H-NMR (500 MHz, D_2O) δ [ppm]: 1.17 (s, 6H, CH_3), 3.05 (s, 4H, CH_2). $^{13}C\{^1H\}$-NMR (75 MHz, D_2O) δ [ppm]: 21.21 (CH_3), 32.35 (CH_2), 46.83 (C). Single crystals of 2,2-dimethylpropane-1,3-diaminium dichloride (**1a** and **1b**) and of 2,2-dimethylpropane-1,3-diaminium dichloride monohydrate (**2**), suitable for crystal structure analysis were selected directly from the bulk material. The main phase turned out to be **1a**, while **1b** and **2** appear as by-products in small quantities. Since the crystals could not be clearly distinguished from each other morphologically, several single crystals were checked via X-ray diffraction and these were separated into three fractions **1a**, **1b** and **2** by hand based on their lattice parameters and used for further analysis. The ratio of **1a** to the sum of **1b** and **2** is estimated to be five to ten.

2.2. IR-and Raman Spectroscopy

IR spectra of **1a**, **1b** and **2** were recorded with a *PerkinElmer Spectrum Two* FT-IR spectrometer, equipped with a $LiTaO_3$ detector (4000–350 cm^{-1}) and an universal ATR unit [24,25]. IR spectrum of **1a**/**1b** [cm^{-1}]: ν(N−H): ~3045 (sh); ν(C−H): 2895 (s, br); 2710 (m); 2607 (m); 2014 (w); δ(N−H): 1593 (m), 1514 (s); δ(C−H): 1472 (m). IR spectrum of

2 [cm^{-1}]: ν(O−H): 3509, 3439, 3366 (m); ν(N−H): ~3035 (sh); ν(C−H): 2912 (s, br); 2610 (m); 2051 (w); δ(N−H): 1588, 1575 (m), 1512 (s); δ(C−H): 1472, 1459 (m).

Raman spectra of **1a**, **1b** and **2** were recorded with a *Bruker MultiRAM* FT Raman spectrometer, equipped with a Nd:YAG laser (1064 nm) and a InGaAs detector (4000–70 cm^{-1}) [26]. Raman spectrum of **1a**/**1b** [cm^{-1}]: ν(N−H): 3050 (m); ν(C−H): 2978, 2904 (s); 2835 (m); 2735, 2615 (w); δ+(N−H): 1601 (w), 1512 (m); δ(C−H): 1481, 1446 (m); $\delta(CH_2)$: 725 (s). Raman spectrum of **2** [cm^{-1}]: ν(O−H): 3363 (w); ν(N−H): 3066 (m); ν(C−H): 2966, 2900 (s); 2827, 2753 (m); δ(N−H): 1569 (w), 1516 (m); δ(C−H): 1473 (s), 1434 (m); $\delta(CH_2)$: 733 (s).

Assignments were made according to [27,28]. The bands and lines below 1400 cm^{-1} are less instructive and are not listed, with the exception of the characteristic CH_2 rocking mode. The CH_2 rocking mode at ~720 cm^{-1} is IR inactive (see Raman spectra).

A comparison to the IR and Raman spectra of *dmpn* can be found in Figure 2.

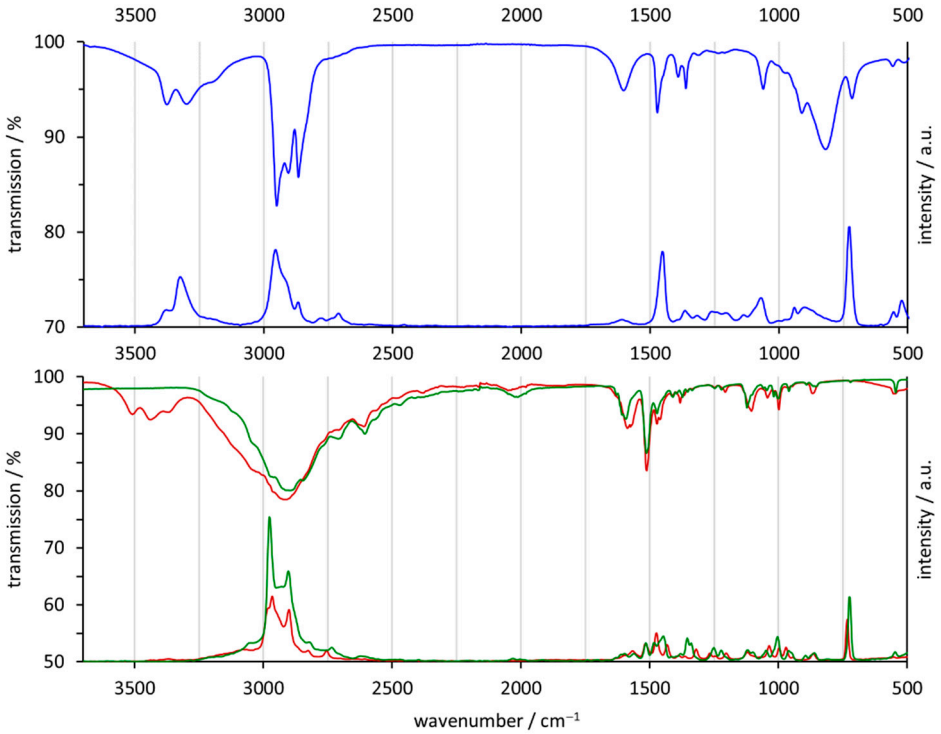

Figure 2. IR and Raman spectra of *dmpn* (blue lines), **1a** (green lines) and **2** (red lines). The IR bands and the Raman lines between 3400 and 3200 cm^{-1} in the spectra of *dmpn* are caused by NH-valence modes of the free amine and are no longer detected in the product spectra. The aminium groups in **1a** and **2** are involved in electrostatically supported hydrogen bonds and the bands of their NH-valence modes are broad and significantly shifted to lower wave numbers, overlapping with the CH-valence modes between 2800 and 3000 cm^{-1}. The presence of water in **2** is indicated by the band of the OH-valence modes between 3600 and 3300 cm^{-1}. The respective signal in the Raman spectrum is of very low intensity.

2.3. Thermal Analysis

Compounds **1a** and **2** were characterized by DSC/TGA thermal analysis. DSC curves were recorded under N_2 atmosphere with a heating/cooling rate of 5 K·min^{-1} in the temperature range of 25–200 °C with a *Mettler-Toledo DSC 1 STAR*^{e} system. The DSC curves of **1a** and **2** (see Figure 3) show a similar appearance except for a series of endothermic features in the range of 55–135 °C, mostly related to the loss of water. The mass of **2** decreases by ~10% (calc. 9.3% for $C_5H_{16}N_2Cl_2$ H_2O). Both compounds, **1a** and **2**, show two further endothermic features in their heating curves at ~138 °C and ~145 °C (peak maxima). The cooling curves each show two exothermic features at ~140 °C and ~125 °C (peak maxima). The shoulder at ~120 °C in the cooling curve of **1a** cannot be clearly assigned

(see Figure 3). These observations suggest at least two reversible phase transitions and a common high-temperature phase of the substances. A TGA curve of the 'dried' material from the DSC measurements was recorded under N_2 atmosphere with a heating rate of 5 K·min^{-1} in the temperature range of 20–600 °C with a *Netsch STA 449C* device. A mass loss of ~98% in the range of 250–400 °C (T_{onset} = 250 °C) is compatible to the complete decomposition of the sample.

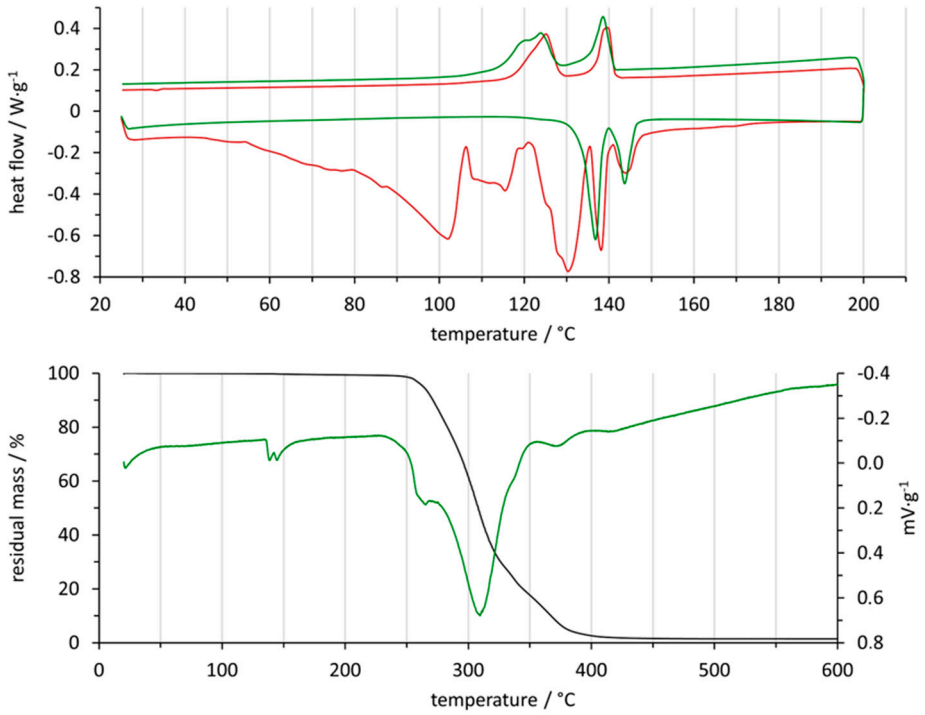

Figure 3. DSC curves (top) of **1a** (green lines) and **2** (red lines) and TGA/DTA curve of the 'dried' material from the DSC measurements (bottom). **2** loses water between 55 and 135 °C and behaves similar to **1a** from this point on. Two reversible phase transitions at ~139 °C and ~145 °C (heating curves) indicate a common high-temperature phase of the substances. The mass loss between 250 and 400 °C is compatible with the complete decomposition of the sample to amine and HCl.

2.4. Crystal Structure Analysis

The single crystal diffraction data of **1a**, **1b,** and **2** were collected with a *Xcalibur Eos* diffractometer. Indexing, unit cell refinement data collection and data processing followed the standard procedures of the *CrysAlisPRO* software package [29]. A multi-scan absorption correction was applied for **1a** and **2** with the SCALE3 ABSPACK routine of *CrysAlisPRO* [29], and an analytical absorption correction was applied for **1b** [30]. The structure solution with Direct Methods and the structure refinement by full-matrix least-squares calculations on F^2 were carried out with programs of the SHLEX family [31–33]. After all non-hydrogen atoms have been located, H atoms bound to C and N were included in idealized positions using a riding model with bond lengths constrained to 0.96, 0.97, and 0.89 Å for CH_3, CH_2 and NH_3, respectively. In addition, the CH_3 and NH_3 groups were allowed to rotate around the adjacent C−C bond. The displacement parameters U_{iso}(H) of the H atoms bound to C and N were set to 1.5U_{eq}, 1.2U_{eq}, and 1.5U_{eq} of the parent atoms for CH_3, CH_2 and NH_3, respectively. Crystals of **1b** and **2** suffered from twinning and were refined as 2-component twins with the HKLF5 option of SHELXL. The fractions of second individual contribution were refined to 0.335 and 0.404 for **1b** and **2**, respectively. Molecular graphics were generated with DIAMOND [34]. Crystal data, data collection and structure refinement details for **1a**, **1b** and **2** are given in Table 1.

Table 1. Crystal data and structure refinement parameters for **1a**, **1b,** and **2**.

Parameters	**1a**	**1b**	**2**
CCDC depository	1966904	1896779	1966943
Crystal data			
Color/shape	Colorless/block	Colorless/block	Colorless/block
Chemical formula	$C_5H_{16}N_2Cl_2$	$C_5H_{16}N_2Cl_2$	$C_5H_{18}N_2OCl_2$
M_r	175.10	175.10	193.11
Temperature [K]	293 (2)	293 (2)	293 (2)
Wavelength [Å]	Mo K_α 0.71073	Mo K_α 0.71073	Mo K_α 0.71073
Crystal system, space group	Monoclinic, $C2/c$	Monoclinic, Cc	Triclinic, $P\bar{1}$
a,	20.7779 (7),	32.1820 (1),	6.2170 (3),
b,	8.2560 (3),	14.9592 (6),	8.2491 (9),
c [Å]	10.9433 (3)	18.7867 (8)	11.2617 (8)
α,	90,	90,	108.876 (8),
β,	93.800 (3),	125.532 (7),	91.412 (5),
γ [°]	90	90	109.706 (7)
Volume [Å^3]	1873.1 (1)	7360.2 (7)	508.66 (8)
Z	8	32	2
$\rho_{calc.}$ [g·cm^{-3}]	1.24	1.26	1.26
μ [mm^{-1}]	0.63	0.64	0.59
Crystal size (mm^3)	1.09 × 0.76 × 0.53	1.09 × 0.80 × 0.46	0.69 × 0.55 × 0.39
Data collection			
Diffractometer	Oxford Xcalibur Eos	Oxford Xcalibur Eos	Oxford Xcalibur Eos
Absorption correction	Multi-scan (CrysAlisPRO)	Analytical (CrysAlisPRO)	Multi-Scan (CrysAlisPro)
T_{min}, T_{max}	0.800, 1.000	0.596, 0.770	0.798, 1.000
F_{000}	752	3008	208
θ range for data collection [°]	$4.53 \leq \theta \leq 35.11$	$4.12 \leq \theta \leq 27.50$	$2.79 \leq \theta \leq 27.50$
Completeness [%]	99.4	99.6	100.0
No. of collected reflections	15949	57169	7957
No. of independent reflections	4000	16816	7957
No. of observed reflections	3248	15013	6626
R_{int}	0.026	0.020	0.039
Refinement			
R values [$F^2 > 2\sigma(F^2)$]	$R_1 = 0.032$, $wR_2 = 0.069$	$R_1 = 0.030$, $wR_2 = 0.065$	$R_1 = 0.043$, $wR_2 = 0.096$
R values (all data)	$R_1 = 0.044$, $wR_2 = 0.075$	$R_1 = 0.036$, $wR_2 = 0.069$	$R_1 = 0.052$, $wR_2 = 0.102$
S (Goodness-of-fit)	1.04	1.06	1.09
No. of data (m)	4000	16816	7957
No. of parameters (n)	108	703	99
No. of restraints	0	2	0
$\Delta\rho_{max}$, $\Delta\rho_{min}$	0.44, −0.32	0.30, −0.33	0.48, −0.50

$R_1 = \Sigma||F_o| - |F_c|| \div \Sigma|F_o|$; $wR_2 = [\Sigma\, w(F_o^2 - F_c^2)^2 \div \Sigma\, w(F_o^2)^2]^{-1/2}$; $S = [\Sigma\, w(F_o^2 - F_c^2)^2 \div (m - n)]^{-1/2}$; $w = 1 \div \sigma^2(F_o^2) + (aP)^2 + bP$; $P = (F_o^2 + 2F_c^2) \div 3$. Weighting factor a for **1a**, **1b** and **2**: 0.02, 0.02, 0.01. Weighting factor b for **1a**, **1b** and **2**: 1.30, 5.00, 0.60. CCDC 1896779, 1966904 and 1966943 contain the supplementary crystallographic data for this paper. These data can be obtained free of charge via http://www.ccdc.cam.ac.uk/conts/retrieving.html (accessed on 1 April 2022) (or from the CCDC, 12 Union Road, Cambridge CB2 1EZ, UK; Fax: +44 1223 336033; E-mail: deposit@ccdc.cam.ac.uk).

3. Results

3.1. Structural Commentary

Compound **1a** crystallizes in the monoclinic space group $C2/c$ ($Z = 8$). The asymmetric unit contains one *dmpn* cation [$(dmpnH_2)^{2+}$] and two chloride anions (all in general positions). The structure forms layers along the crystallographic *a*-axis (see Figure 4). Each layer consists of strands, each of which contains two symmetry related cations arranged around a center of inversion. Both aminium groups of the cations and the chloride anions are involved into a N−H···Cl hydrogen-bonded network. The geometrical parameters of all hydrogen bonds are given in Table 2. All N···Cl distances are in narrow ranges of 3.146 (1)–3.180 (1) Å [35]. There are others in the range of 3.272 (1)–3.336 (1) Å which are significantly weaker. Obviously, the cations show an unsymmetrical hydrogen bonding pattern. The aminium group including N1 forms three hydrogen bonds to chloride anions

within the same strand. The aminium group including N2 forms one hydrogen bond to a chloride anion within the same strand and one hydrogen bond to the adjacent strand, causing the connection between the strands. No N−H···Cl hydrogen bonds could be identified between adjacent layers along the crystallographic *a*-axis. Consequently, they are connected by van der Waals forces and non-classical C−H···Cl hydrogen bonds.

Compound **2** crystallizes in the triclinic space group $P\bar{1}$ (Z = 2). The asymmetric unit contains one cation [(*dmpn*H_2)$^{2+}$] and two chloride anions (all in general positions). Four symmetry related formula units each form a cavity with two water molecules inside (see Figure 4). These two water molecules build a dimer arranged around a center of inversion in the middle of the cavity. They are connected by a classical O−H···O hydrogen bond with a O1···O2 distance of 2.776 (8) Å. Thus, the cavity is too large for only one water dimer the structure refinement suggests that there are two energetically identical positions for this water dimer which are each half occupied. In general, eight hydrogen bonds caused by aminium groups, and three hydrogen bonds caused by the water molecules can be identified. The geometrical parameters of these hydrogen bonds are given in Table 1. All N···Cl distances are in narrow ranges of 3.173 (2)–3.318 (3) Å [35]. The hydrogen bonds of N1–H11 and N2–H22 are bifurcated and their N···Cl distances are significantly longer than those of the other ones. The half-occupied water molecules including O1 and O2 each form two O−H···Cl hydrogen bonds with chloride anions.

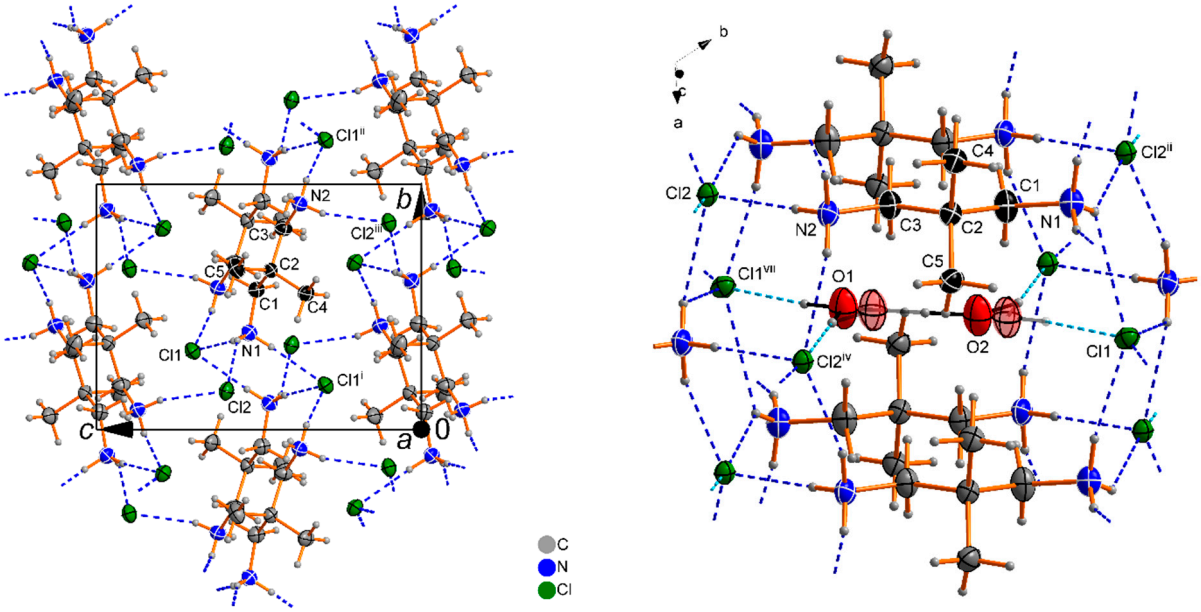

(**a**) (**b**)

Figure 4. Sections of the crystal structures, showing the layered arrangement of *dmpn*H_2Cl_2 along the crystallographic *a*-axis in **1a** (**a**), and the cavity containing a water dimer in **2** (**b**). Displacement ellipsoids are drawn at the 50% probability level; H atoms are drawn with an arbitrary radius. The direction of hydrogen bonds is given by blue dotted lines; the direction of further N−C bonds by truncated sticks. For the sake of clarity, the C atoms belonging to the chosen asymmetric unit are drawn in black. [Symmetry codes for **1a**: (i) $^1/_2-x$, $^1/_2-y$, 1−z; (ii) $^1/_2-x$, $^3/_2-y$, 1−z; (iii) x, 1−y, $z-^1/_2$. Symmetry codes for **2**: (i) 1−x, −y, 1−z; (ii) 1−x, 1−y, 2−z; (iii) −x, −y, 1−z; (iv) 1−x, 2−y, 2−z; (v) 1−x, 1−y, 1−z; (vi) 2−x, 2−y, 2−z; (vii) x, y+1, z; (viii) −x, 1−y, 1−z]. In **1a** two symmetry-related (*dmpn*H_2)$^{2+}$ cations each are arranged around a center of inversion (*4c* Wyckoff site). The strands are connected by N−H···Cl hydrogen bonds while adjacent layers (viewing direction) are connected by non-classical C−H···Cl hydrogen bonds and van der Waals forces.

Table 2. Hydrogen-bond geometry (Å, °) for **1a** and **2**.

D-H···A	D-H	H···A	D···A	D-H···A
Compound **1a**				
N1-H11···Cl1	0.87 (2)	2.30 (2)	3.1619 (9)	170 (2)
N1-H12···Cl2	0.89 (2)	2.35 (2)	3.146 (1)	148 (1)
N1-H13···Cl1^{i}	0.90 (2)	2.27 (2)	3.163 (1)	175 (1)
N2-H21···Cl2^{iv}	0.76 (2)	2.66 (2)	3.183 (1)	128 (2)
N2-H22···Cl1^{ii}	0.88 (2)	2.49 (2)	3.272 (1)	149 (2)
N2-H23···Cl2^{iii}	0.87 (2)	2.33 (2)	3.180 (1)	165 (2)
Compound **2**				
N1-H11···Cl1^{i}	0.89	2.66	3.234 (2)	122.9
N1-H11···Cl2^{ii}	0.89	2.68	3.245 (2)	122.5
N1-H12···Cl1	0.89	2.31	3.195 (2)	174.3
N1-H13···Cl1^{iii}	0.89	2.35	3.173 (2)	153.7
N2-H21···Cl2^{iv}	0.89	2.33	3.206 (3)	169.2
N2-H22···Cl1^{v}	0.89	2.57	3.223 (2)	131.2
N2-H22···Cl2^{vi}	0.89	2.80	3.318 (3)	118.7
N2-H23···Cl2	0.89	2.39	3.189 (2)	149.0
O1-H1O···Cl2^{iv}	1.05	2.22	3.259 (6)	175.7
O1-H2O···Cl1^{vii}	0.91	2.22	3.136 (7)	177.6
O2-H3O···O1	1.09	1.69	2.776 (8)	177.5

Symmetry codes for **1a**: (i) $^{1}/_{2}-x$, $^{1}/_{2}-y$, $1-z$; (ii) $^{1}/_{2}-x$, $^{3}/_{2}-y$, $1-z$; (iii) x, $1-y$, $z-^{1}/_{2}$; (iv) x, $1+y$, z. Symmetry codes for **2**: (i) $1-x$, $-y$, $1-z$; (ii) $1-x$, $1-y$, $2-z$; (iii) $-x$, $-y$, $1-z$; (iv) $1-x$, $2-y$, $2-z$; (v) $1-x$, $1-y$, $1-z$; (vi) $2-x$, $2-y$, $2-z$; (vii) x, $y+1$, z; (viii) $-x$, $1-y$, $1-z$.

3.2. Conformational Analysis

A theoretical conformational analysis of the 2,2-dimethylpropane-1,3-diaminium cation was performed. As shown in Figure 5, six conformations can be postulated for the rotation of the amino group including N1 around the N1C1–C2C3 bond. The eclipsed conformations with the dihedral torsion angle Θ at 0° (*syn*), +120° and −120° (=+240°) are conformers with maximum energies. The staggered conformations with Θ at +60° (*gauche*) and −60° (=+300°) as well as 180° (*anti*) are conformers with minimum energies. Assuming that the two amino groups do not interact with each other, the same ideas can be applied for the rotation of the amino group including N2 around the C1C2−C3N2 bond.

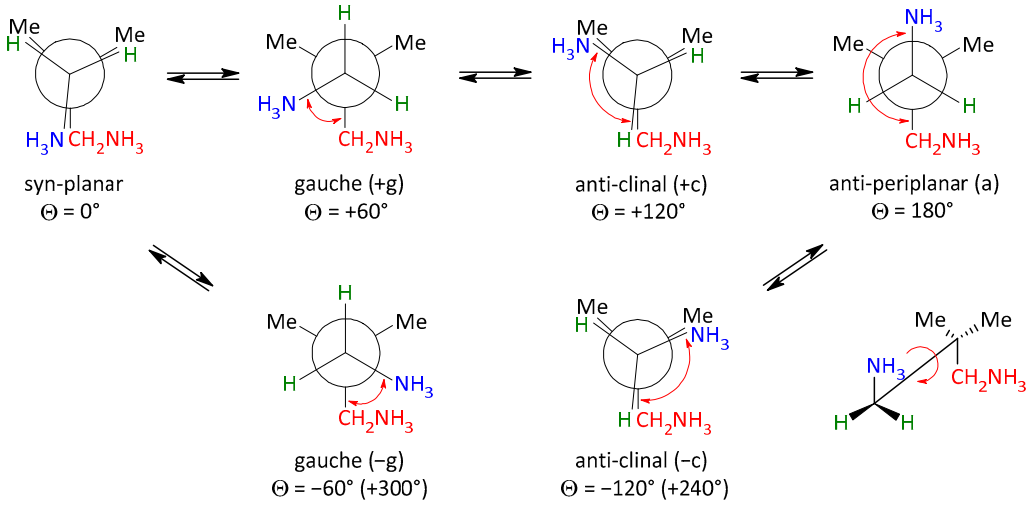

Figure 5. Newman projections for possible conformations of the 2,2-dimethylpropane-1,3-diaminium cation resulting by the rotation of the amino groups including N1 and N2 around the C1–C2 bond and the C2–C3 bond, respectively. The anti-periplanar conformation is expected to be the most stable conformation with minimum energy.

In order to get a qualitative impression of the energy landscape for the rotation of the two amino groups in the $(dmpnH_2)^{2+}$ cation, quantum chemical calculations have been performed. The *Turbomole* [36] suite of programs was used at the density functional theory (DFT) level with B3-LYP functional and the def-SV(P) basis set in the gas phase. Constrained geometry optimizations have been performed on a 2-dimensional grid. The N1C1–C2C3 angle has been scanned from 0 to 360° in steps of 5°, the C1C2−C3N2 angle from 20 to 180° in steps of 5° (10° in the range of 20–50°). The values for this angle from 180 to 340° have been obtained by symmetry. The scan reveals the *anti-anti*-conformation [Θ_1/Θ_2: 180°/180° (aa)] to be the global minimum (see Figure 6). In this conformation, the atoms N1, C1, C2, C3, and N2 are all in-plane. Barriers of 21 kJ·mol^{-1} (read from the grid) lead to four equivalent local minima for the *anti-gauche*-conformations [Θ_1/Θ_2: 180°/+60° (ag), 180°/−60° (a–g), +60°/180° (ga), −60°/180° (−ga)]. These correspond to one of the amino groups being turned up or down from the C1-C2-C3 plane. An unconstrained optimization of these structures yields angles of 173°/76° and an energy of 13 kJ·mol^{-1} above the conformational ground state. Inspecting the four *gauche-gauche*-combinations [Θ_1/Θ_2: +60°/+60° (gg), +60°/−60° (g–g), −60°/+60° (–gg), −60°/−60° (–g–g)], two pairs of equivalent structures can be found. The first pair corresponds to turning the two amino groups in opposite directions. An optimization puts this conformation at 80.1°/80.1°, 25 kJ·mol^{-1} above the conformational ground state. The barrier connecting these g/g minima to the a/g minima is at 31 kJ·mol^{-1} above the conformational ground state or only 6 kJ·mol^{-1} above the g/g minimum. The second pair corresponds to both amino groups turned in the same direction. Here, no minimum is found on the grid but only a saddle point at 100°/270°, 52 kJ·mol^{-1} above the conformational ground state.

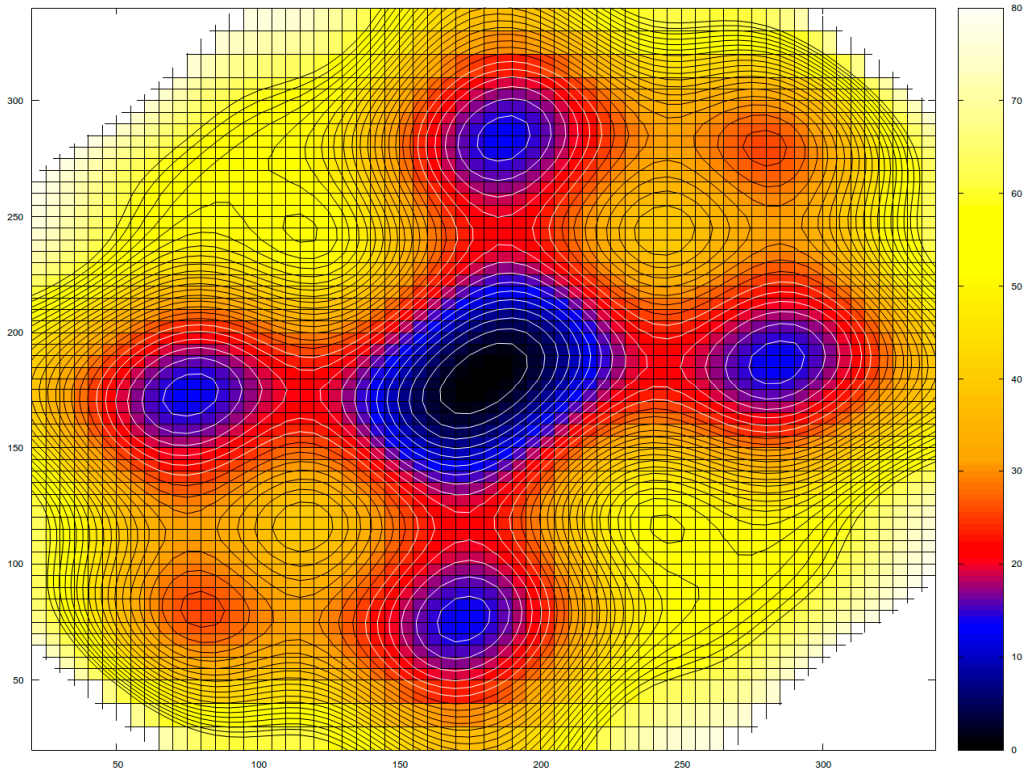

Figure 6. Potential energy surface for the rotation of the two amino groups in the $(dmpnH_2)^{2+}$ cation, obtained by quantum chemical calculations, showing a global minimum for the *anti-anti*-conformer (0 kJ·mol^{-1}), a set of four equivalent local minima for the *anti-gauche*-conformers (13 kJ·mol^{-1}), a set of two equivalent local minima for the *gauche-gauche*-conformers (25 kJ·mol^{-1}) with the two amino groups oriented in opposite directions, and finally two saddle points for the *gauche-gauche*-conformers (52 kJ·mol^{-1}) with the two amino groups oriented in the same direction.

The experimental torsion angles of the $(dmpnH_2)^{2+}$ cation in the crystal structures of $dmpnH_2Cl_2$ (**1a** and **1b** [19]), $dmpnH_2Cl_2{\cdot}H_2O$ (**2**), $dmpnH_2Br_2$ [11], $dmpnH_2I_2$ [11], $dmpnH_2I_2I_2$ [12], $dmpnH_2(NO_3)_2$ [13], $dmpnH_2(CrO_4)$ [14], $dmpnH_2[ZnCl_4]$ [15], $dmpnH_2[CdBr_4]$ [16] and $dmpnH_2[InBr_4][InBr_{11}]$ [17] are summarized in Table 3.

Table 3. Torsion angles (°) and conformations of the $(dmpnH_2)^{2+}$ cation in experimental structures.

Compound	Θ_1	Θ_2	Conformation	Reference
$C_5H_{16}N_2Cl_2$ (**1a**)	169.77 (9)	−178.15 (9)	aa	
$C_5H_{16}N_2Cl_2$ (**1b**)	−174.0 (4)	76.0 (5)	ag	[19]
	54.3 (6)	174.5 (4)	ga	
	174.1 (4)	49.7 (6)	ag	
	76.4 (5)	−174.1 (4)	ga	
	54.1 (7)	172.2 (5)	ga	
	74.9 (5)	−173.4 (4)	ga	
	72.3 (5)	−174.1 (4)	ga	
	52.7 (6)	175.6 (4)	ga	
$C_5H_{16}N_2Cl_2{\cdot}H_2O$ (**2**)	176.8 (2)	−171.2 (2)	aa	
$C_5H_{16}N_2Br_2$	−171.2 (5)	177.7 (5)	aa	[11]
$C_5H_{16}N_2I_2$	−71 (1)	−71 (1)	gg	[11]
$C_5H_{16}N_2I_2{\cdot}I_2$	180.0 (3)	180.0 (3)	aa	[12]
$C_5H_{16}N_2$ $(NO_3)_2$	−58.8 (2)	−64.0 (2)	gg	[13]
$C_5H_{16}N_2$ $[CrO_4]$	−178.3 (2)	−169.0 (2)	aa	[14]
$C_5H_{16}N_2$ $[ZnCl_4]$	176.38 (8)	165.16 (8)	aa	[15]
$C_5H_{16}N_2$ $[CdBr_4]$	74.6 (8)	−176.2 (8)	ga	[16]
$(C_5H_{16}N_2)_3$ $[InBr_4]$ $[In_2Br_{11}]$	−170 (1)	−177 (1)	aa	[17]
	178.2 (6)	74.4 (8)	ag	
	178.4 (6)	70.3 (8)	ag	

Abbreviations for the conformations of the $(dmpnH_2)^{2+}$ cation are used as follows: anti-periplanar (a); gauche (g); anti-clinal (c); rotation of N1C1–C2C3 (Θ_1) rotation of C1C2–C3N2 (Θ_2).

3.3. Topological Classification

The aminium groups together with the chloride ions form supramolecular hydrogen bonded networks in their crystal structures. Using the ToposPro software package [37] the topology of these networks can be classified using the concept of the simplified underlying net [38]. Figure 7a shows the simplified network of **1a**, which can be assigned to the class *cbs/CrB* (chromium boride type) [37,39,40]. Three different types of interconnected strands can be identified, which are colored orange, blue and pink for discussion. Each strand consists of distorted rectangles, each formed by two N and two Cl atoms. The arrangement guaranties alternating occurrence of aminium groups and chloride anions. Thus, each N atom is surrounded by four Cl atoms and *vice versa*. The rectangles within a strand are folded in a stair-like manner. The orange-colored strands are crossed by the pink- and the blue-colored strands, while pink- and blue-colored strands never cross (see Figure 7a). Figure 7b shows the simplified network of **2**. The topological net can be assigned to the class *tcs* (thorium chromium silicide type) [41–47]. It consists of two different types of dodecahedra, which are colored orange and blue for discussion. These polyhedra show a significant distortion of their hexagonal faces, whose angles deviate from the ideal value of 120°. While the orange-colored polyhedra are stretched along the crystallographic *c*-axis with an N···Cl···N angle of 147.2°, the angle for the blue-colored polyhedra is 108.1°. The individual disorder of the water dimers contained in the blue-colored polyhedra seems to be determined by the fact that this type of polyhedra is elongated along the crystallographic *b*-axis. Within one layer, polyhedra of the same type form a columnar connection pattern, where the connection is established by the hexagonal faces along the crystallographic *a*-axis. Along the crystallographic *c*-axis, the polyhedron types alternate and are connected by further hexagonal faces (see Figure 7b).

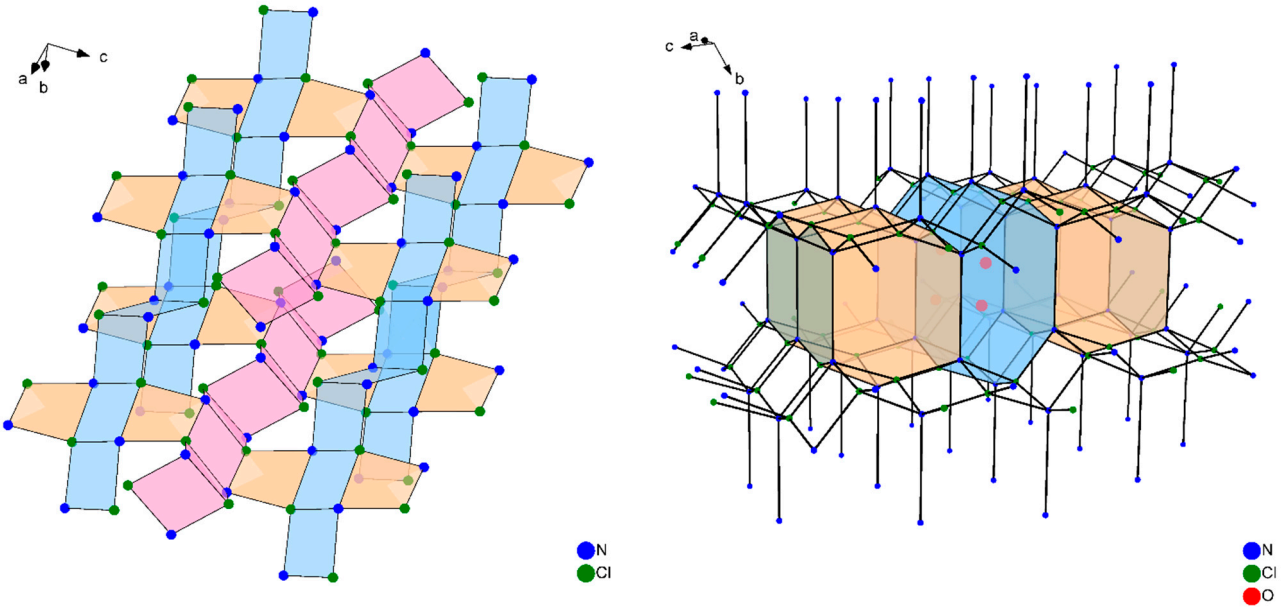

(**a**) (**b**)

Figure 7. Topological nets, showing three different kinds of connected strands in **1a** (**a**), and two types of connected dodecahedra in **2** (**b**). For the sake of clarity, only N, Cl, and O atoms are shown. The topological nets can be assigned to the classes *cbs/CrB* (chromium boride type) and *tcs* (thorium chromium silicide type) in the case **1a** and **2**, respectively.

4. Conclusions

In this work, two new salts in the *dmpn*/HCl/H_2O-system have been synthesized and characterized by crystal structure analysis, spectroscopic methods, thermal analysis, and topological classification. Thus, the series of reported halide salts of *dmpn* has been extended. Phases **1a** and **2** show reversible phase transformations at the same temperatures, indicating that a common high-temperature phase of them exists. This could hold potential for further research. A comparison of the crystal structures of **1a**, **1b**, **2** and further salts from the CSD [18], revealed that the energetically favorable *anti-anti*-conformer is not always the best option for the 2,2-dimethylpropane-1,3-diaminium cation in the solid state [11–17,19]. The conformational analysis, which was supported by quantum chemical calculations, verified that the *anti-anti*-conformation represents the global minimum on the potential energy surface. In some cases, the *anti-gauche*- and the *gauche-gauche*-conformation are preferred (see Table 3), obviously due to the formation of hydrogen bonds within the corresponding solid-state structures. The most interesting finding is certainly the caging of water dimers in **2**. This particular property of the *dmpn*/HX/H_2O-system may enable the caging of other small molecules such as Br_2, IF, IBr, and ICl. By using aliphatic diamines with extended alkyl chains, it might be possible to enlarge the cavity observed in **2** to cage polyiodide chains, such as $[I_6]^{2-}$ [48].

Author Contributions: G.J.R. initialized and supervised this project; J.H. and F.M. realized the experiments and prepared the original draft of the manuscript; M.K. performed the quantum chemical calculations. All authors, J.H., F.M., M.K. and G.J.R., contributed significantly to the final draft of the manuscript. All authors have read and agreed to the published version of the manuscript.

Funding: Deutsche Forschungsgemeinschaft: INST 208/533-1, project no. 162659349; Open-Access-Fonds of Heinrich-Heine-University Düsseldorf: ULBD-22-.

Acknowledgments: The authors thank Eleonore Hammes, Peter Roloff and Daniel Mombers for technical support.

Conflicts of Interest: The authors declare no conflict of interest.

References

1. Senkus, M. Iron reduction of some aliphatic nitro compounds. *J. Ind. Eng. Chem.* **1948**, *40*, 506–508. [CrossRef]
2. Feichtinger, H.; Aschmann, H.; Birnkraut, H.-W.; Brinkmann, L.; Pluta, W. Method for the Preparation of 1,3-Diamino-2,2-Dimethyl Propane. U.S. Patent US4078003A, 1973.
3. Hares, G.B.; Fernelius, W.C.; Douglas, B.E. Equilibrium constants for the formation of complexes between metal ions and polyamines. *J. Am. Chem. Soc.* **1956**, *78*, 1816–1818. [CrossRef]
4. Skinner, G.S.; Wunz, P.R. 2,5,5-Trialkyl-l,4,5,6-tetrahydropyrimidines. *J. Am. Chem. Soc.* **1951**, *73*, 3814–3815. [CrossRef]
5. Fleischer, E.B.; Gebala, A.E.; Levey, A.; Tasker, P.A. Conversion of aliphatic and alicyclic polyalcohols to the corresponding primary polyamines. *J. Org. Chem.* **1971**, *36*, 3042–3044. [CrossRef]
6. Kim, H.; Kim, Y.K.; Shim, J.H.; Kim, M.; Han, M.; Livinghouse, T.; Lee, P.H. Internal alkene hydroaminations catalyzed by Zirconium(IV) complexes and asymmetric alkene hydroaminations catalyzed by Yttrium(III) complexes. *Adv. Synth. Catal.* **2006**, *348*, 2609–2618. [CrossRef]
7. Biswas, A.; Jana, A.; Sarkar, S.; Sparkes, H.A.; Howard, J.A.K.; Aliaga-Alcalde, N.; Mohanta, S. Discrete systems and two-dimensional coordination polymers containing potentially multidentate and bridging inorganic anions: Observation of a new type of two-dimensional topology. *Polyhedron* **2014**, *74*, 57–66. [CrossRef]
8. Milner, P.J.; Siegelman, R.L.; Forse, A.C.; Gonzalez, M.I.; Runcevski, T.; Martell, J.D.; Reimer, J.A.; Long, J.R. A diaminopropane-appended metal−organic framework enabling efficient CO_2 capture from coal flue gas via a mixed adsorption mechanism. *J. Am. Chem. Soc.* **2017**, *139*, 13541–13553. [CrossRef]
9. Heimgert, J.; Neumann, D.; Reiss, G.J. (3-Ammonio-2,2-dimethyl-propyl)carbamate dihydrate. *Molbank* **2018**, *2018*, M1015. [CrossRef]
10. Alam, M.; Kim, Y.; Park, S. Quantum chemical calculations, spectroscopic studies and biological activity of organic–inorganic hybrid compound (2,2-dimethylpropane-1,3-diammonium) tetrachlorozincate(II). *Arab. J. Sci. Eng.* **2019**, *44*, 631–645. [CrossRef]
11. Dou, S.; Fuess, H.; Paulus, H.; Weiss, A. Halogen NQR and crystal structure of ammonium halides $(R\text{-}NH_3)^+X^-$ and $(X^-)(^+H_3NR'NH_3^+)(X^-)$. R=$(HOCH_2)_3C$, R'=$CH_2C(CH_3)_2CH_2$; X=I, Br *. *Z. Naturforsch.* **1994**, *49*, 174–184. [CrossRef]
12. Megen, M.v.; Jablonka, A.; Reiss, G.J. Synthesis, structure and thermal decomposition of a new iodine inclusion compound in the 2,2-dimethylpropane-1,3-diamine/HI/I_2 System. *Z. Naturforsch.* **2014**, *69*, 753–760. [CrossRef]
13. Reiss, G.J.; Heimgert, J.; Morsbach, F. CCDC 1901965: Experimental Crystal Structure Determination. 2019. Available online: https://www.ccdc.cam.ac.uk/structures/search?id=doi:10.5517/ccdc.csd.cc21nrfx&sid=DataCite (accessed on 1 April 2022).
14. Chebbi, H.; Hajem, A.A.; Driss, A. Chromate de 2,2-diméthylpropyléne-diammonium. *Acta Cryst. C* **2000**, *56*, e333–e334. [CrossRef]
15. Al-Resayes, S.I.; Azam, M.; Alam, M.; Kumar, R.S.; Adil, S.F. Synthesis, crystal structure and Hirschfeld surface analyses of an alkyl amine based salt, $[C_5H_{16}N_2][ZnCl_4]$ and its enzyme inhibition activity. *J. Saudi Chem. Soc.* **2017**, *21*, 481–486. [CrossRef]
16. Ishihara, H.; Dou, S.; Horiuchi, K.; Krishnan, V.G.; Paulus, H.; Fuess, H.; Weiss, A. Isolated versus condensed anion structure: The influence of the cation size and hydrogen bond on structure and phase transition in MX_4^{2-} complex salts. 2,2-dimethyl-1,3-propanediammonium tetrabromocadmate(II) monohydrate, dimethylammonium tetrabromozincate(II), and dimethylammonium tetrabromocadmate(II). *Z. Naturforsch.* **1996**, *51*, 1027–1036.
17. Iwakiri, T.; Terao, H.; Lork, E.; Gesing, T.M.; Ishihara, H. X-ray and NQR studies of bromoindate(III) complexes: $[C_2H_5NH_3]_4InBr_7$, $[C(NH_2)_3]_3InBr_6$, and $[H_3NCH_2C(CH_3)_2CH_2NH_3]InBr_5$. *Z. Naturforsch.* **2017**, *72*, 141–151. [CrossRef]
18. Allen, F.H. The Cambridge Structural Database: A quarter of a million crystal structures and rising. *Acta Cryst.* **2002**, *58*, 380–388. [CrossRef]
19. Reiss, G.J.; Heimgert, J.; Morsbach, F. CCDC 1896779: Experimental Crystal Structure Determination. 2019. Available online: https://www.ccdc.cam.ac.uk/structures/search?id=doi:10.5517/ccdc.csd.cc21nrfx&sid=DataCite (accessed on 1 April 2022).
20. Lemmerer, A.; Fernandes, M.A. Adventures in co-crystal land: High Z′, stoichiometric variations, polymorphism and phase transitions in the co-crystals of four liquid and solid cyclic carboxylic acids with the supramolecular reagent isonicotinamide. *New J. Chem.* **2012**, *36*, 2242–2252. [CrossRef]
21. Lemmerer, A.; Bernstein, J.; Spackman, M.A. Supramolecular polymorphism of the 1:1 molecular salt (adamantane-1-carboxylate-3,5,7-tricarboxylic acid)·(hexamethylenetetraminium). A "failed" crystal engineering attempt. *Chem. Commun.* **2012**, *48*, 1883–1885. [CrossRef]
22. *vario MICRO 3.1.12*, Elementar Analysesysteme GmbH: Langenselbold, Germany, 2015.
23. *MestReNova 14.2.0*, Mestrelab Research S.L.: Santiago de Compostela, Spain, 2015.
24. *Spectrum 10™*, PerkinElmer Inc.: Waltham, MA, USA, 2008.
25. Feustel, M. *Grundlagen der ATR-Technik*; Resultec Analytical Equipment: Illerkirchberg, Germany, 1999.
26. *OPUS 6.5*, Bruker Corp.: Billerica, MA, USA, 2009.
27. Bienz, S.; Bigler, L.; Fox, T.; Meier, H. *Spektroskopische Methoden in der Organischen Chemie*, 9th ed.; Georg Thieme Verlag: Stuttgart, Germany, 2016.
28. Kowalczyk, I. Synthesis, molecular structure and spectral properties of quaternary ammonium derivatives of 1,1-dimethyl-1,3-propylenediamine. *Molecules* **2008**, *13*, 379–390. [CrossRef]
29. *CrysAlisPRO 1.171.34.44*; Oxford Diffraction Ltd.: Abingdon, UK, 2011.
30. Clark, R.C.; Reid, J.S. The analytical calculation of absorption in multifaceted crystals. *Acta Cryst.* **1995**, *51*, 887–897. [CrossRef]

31. Hübschle, C.B.; Sheldrick, G.M.; Dittrich, B. A Qt graphical user interface for SHELXL. *J. Appl. Crystallogr.* **2011**, *44*, 1281–1284. [CrossRef] [PubMed]
32. Sheldrick, G.M. Crystal structure refinement with SHELXL. *Acta Crystallogr.* **2015**, *71*, 3–8.
33. Sheldrick, G.M. SHELXT-Integrated space-group and crystal-structure determination. *Acta Crystallogr.* **2015**, *71*, 3–8. [CrossRef] [PubMed]
34. Brandenburg, K. *DIAMOND 4.6.4*, Crystal Impact GbR: Bonn, Germany, 2018.
35. Steiner, T. Hydrogen-bond distances to halide ions in organic and organometallic crystal structures: Up-to-date database study. *Acta Cryst.* **1998**, *54*, 456–463. [CrossRef]
36. TURBOMOLE. *Program Package for ab Initio Electronic Structure Calculations. V7.1*; 1989–2007, TURBOMOLE GmbH, since 2007; University of Karlsruhe and Forschungszentrum Karlsruhe GmbH: Karlsruhe, Germany, 2016.
37. Blatov, V.A.; Shevchenko, A.P.; Proserpio, D.M. Applied topological analysis of crystal structures with the program package ToposPro. *Cryts. Growth Des.* **2014**, *14*, 3576–3586. [CrossRef]
38. Blatov, V.A. Multipurpose crystallochemical analysis with the program package TOPOS. *IUCr CompComm Newsl.* **2006**, *7*, 4–38.
39. Kirillova, M.V.; Santos, C.I.M.; André, V.; Fernandes, T.A.; Dias, S.S.P.; Kirillov, A.M. Self-assembly generation, structural features, and oxidation catalytic properties of new aqua-soluble copper(II)-aminoalcohol derivatives. *Inorg. Chem. Front.* **2017**, *4*, 968–977. [CrossRef]
40. Blatov, V.A.; Proserpio, D.M. Topological relations between three-periodic nets. II. Binodal nets. *Acta Cryst.* **2009**, *65*, 202–212. [CrossRef]
41. Kumar, M.; Qiu, C.-Q.; Zareba, J.K.; Frontera, A.; Jassal, A.K.; Sahoo, S.C.; Liu, S.-J.; Sheikh, H.N. Magnetic, luminescence, topological and theoretical studies of structurally diverse supramolecular lanthanide coordination polymers with flexible glutaric acid as a linker. *New J. Chem.* **2019**, *43*, 14546–14564. [CrossRef]
42. Jansen, C.; Küper, J.; Krebs, B. $Na_2B_2S_5$ and $Li_2B_2S_5$: Two novel perthioborates with planar 1,2,4-trithia-3,5-diborolane rings. *Z. Anorg. Allg. Chem.* **1995**, *621*, 1322–1329. [CrossRef]
43. Löhken, A.; Mewis, A. Crystal Structures of $Ca_4Ir_8P_7$ and $Ca_4Ir_8As_7$ and the Relationship to the $ThCr_2Si_2$ Type Structure. *Z. Anorg. Allg. Chem.* **2004**, *630*, 2418–2421. [CrossRef]
44. Ban, Z.; Sikirica, M. The crystal structure of ternary silicides ThM_2Si_2 (M=Cr, Mn, Fe, Co, Ni and Cu). *Acta Cryst.* **1965**, *18*, 594–599. [CrossRef]
45. Pfannenschmidt, U.; Rodewald, U.C.; Pöttgen, R. $Ce_{13}Ir_{34.4}P_{24}$–An intergrowth structure of $ThCr_2Si_2$, SrPtSb, and $CeMg_2Si_2$ related slabs. *Z. Kristallogr.* **2011**, *226*, 229–235. [CrossRef]
46. Seidel, S.; Hoffmann, R.-D.; Pöttgen, R. $SrPdGa_3$–An orthorhombic superstructure of the $ThCr_2Si_2$ type. *Z. Kristallogr.* **2014**, *229*, 421–426. [CrossRef]
47. Hellmann, A.; Löhken, A.; Wurth, A.; Mewis, A. Neue Arsenide mit $ThCr_2Si_2$- oder einer damit verwandten Struktur: Die Verbindungen ARh_2As_2 (A: Eu, Sr, Ba) und $BaZn_2As_2$. *Z. Naturforsch.* **2007**, *62*, 155–161. [CrossRef]
48. Van Megen, M.; Reiss, G.J. I_6^{2-} anion composed of two asymmetric triiodide moieties-A competition between halogen and hydrogen bond. *Inorganics* **2013**, *1*, 3–13. [CrossRef]